Satellite observations of banded VLF emissions in conjunction with energy-banded ions during very large geomagnetic storms

Christopher A. Colpitts,[1] Cynthia A. Cattell,[1] Janet U. Kozyra,[2] and Michel Parrot[3]

Received 2 November 2011; revised 4 September 2012; accepted 5 September 2012; published 10 October 2012.

[1] Frequency-banded electromagnetic VLF waves up to 2000 Hz are observed concurrently with warm (10 s to 10,000 s of eV) energy-banded ions in the low latitude auroral and sub-auroral zones during every large geomagnetic storm encountered by the FAST and DEMETER satellites. The banded ions and waves persist for several FAST or DEMETER orbits, lasting up to 12 h, in both dawn and dusk sectors, in both the northern and southern hemispheres. If the waves are generated at harmonics of the proton gyrofrequency, the inferred source region would be ~4000 km altitude. Previous investigations have shown that such waves can propagate from this source region to the locations of both spacecraft. An investigation into the growth of waves at harmonics of f_{ci} in the inferred source region suggests that these emissions could be generated by ion bands similar to those observed at the same time as the waves. Magnetospheric waves such as these play a role in energy transfer between distinct particle populations and may contribute to ion heating and ion outflow as well as electron energization. All of these phenomena occur during the strongest magnetic storms. The appearance of the banded ions and associated wave activity suggests that there may be distinct changes in the geospace system that characterize large magnetic storms.

Citation: Colpitts, C. A., C. A. Cattell, J. U. Kozyra, and M. Parrot (2012), Satellite observations of banded VLF emissions in conjunction with energy-banded ions during very large geomagnetic storms, *J. Geophys. Res.*, *117*, A10211, doi:10.1029/2011JA017329.

1. Introduction

[2] Banded VLF emissions are commonly observed in the inner magnetosphere and are typically interpreted as harmonics of either an artificial transmission frequency or a fundamental resonance such as the ion (or electron) gyrofrequency or plasma frequency. In addition to the well-documented ion cyclotron harmonics [*Kintner*, 1980; *Koskinen et al.*, 1987; *Chaston et al.*, 2002], these banded emissions include VLF chorus [*Burtis and Helliwell*, 1969], VLF Hiss [*Titova et al.*, 2007], Power Line Harmonic Radiation [*Němec et al.*, 2006], and Magnetic Line Radiation [*Němec et al.*, 2009] among others. In the low altitude auroral region, waves at harmonics of the ion cyclotron frequency have been observed with FAST in association with both downgoing [*Cattell et al.*, 2002] and upgoing [*Chaston et al.*, 2002] ion beams. Different types of banded emissions are observed during quiet, active, and storm times; from here on we focus on storm time observations. *Liu et al.* [1994] observed emissions near oxygen cyclotron harmonics with the Akebono satellite during very strong storms, in the morning sector in the low altitude plasmasphere (L = 1.5 ~ 2.5).

[3] Ions banded in energy have been observed on auroral field lines from satellites at low-, mid-, and high-latitudes. Most recently, Cluster has observed ions in narrow energy bands within the plasmasphere [*Dandouras et al.*, 2009]. In the low altitude auroral zone, energy-banded ions have been observed during quiet times, interpreted as either convective drift dispersion [*Hirahara et al.*, 1997] or time-of-flight dispersion [*Boehm et al.*, 1999]. Warm (10 s to 10,000 s of eV) energy-banded ions in the low latitude auroral zone, coincident with electromagnetic emissions banded in frequency, and associated with very strong geomagnetic storms, represent an entirely new phenomenon. These ion bands were first reported in association with the Halloween storms [*Cattell et al.*, 2004; *Kozyra et al.*, 2004; *Huang et al.*, 2005] and were further examined in a statistical study of observations from 2000 [*Yao et al.*, 2008].

[4] The energy-banded ions are an energetically important component of the inner magnetosphere during the most intense magnetic storms. Evidence suggests that the banded ions may be the energy or particle source for many previously reported but unexplained phenomena during superstorms, including unusually intense stable auroral red (SAR) arcs [cf. *Baumgardner et al.*, 2007], intense midlatitude ion-atom auroras [*Zhang et al.*, 2006], and the enhanced low energy (<30 keV) component of the ring current [cf. *Hamilton et al.*,

[1]School of Physics and Astronomy, University of Minnesota, Twin Cities, Minneapolis, Minnesota, USA.
[2]Department of Atmospheric, Oceanic and Space Sciences, University of Michigan, Ann Arbor, Michigan, USA.
[3]Laboratoire de Physique et Chimie de l'Environnement et de l'Espace, Centre National de la Recherche Scientifique, Orléans, France.

Corresponding author: C. A. Colpitts, School of Physics and Astronomy, University of Minnesota, Twin Cities, 476 Tate Laboratory, 116 Church St. SE, Minneapolis, MN 55455, USA. (chrisc@fields.space.umn.edu)

0148-0227/12/2011JA017329

1988]. Protons within the energy range of the banded ions provide an additional major source of Coulomb drag heating of plasmaspheric electrons [*Kozyra et al.*, 1997], not present during smaller storms, and thus a natural explanation for the dramatic intensification of SAR arcs at these times. The charge exchange loss of the energy-banded ions due to collisions with the dense geocorona below 4000 km altitude, and at MLATS as low as 28°, must provide a significant, and possibly the dominant, source of energetic neutral atoms for strong midlatitude ion-atom auroras seen in association with the largest storms. Finally, evidence suggests that the energy-banded ions make a significant contribution to the low-energy portion of the ring current, which is enhanced during superstorms. During the February 1986 superstorm, *Hamilton et al.*, [1988] estimated that 1–30 keV ions contributed 36% of the ring current energy density at storm maximum on the dawn side at L values of 2–3, in the same region and during the same time interval that *Swider* [1990] reported penetration of the precipitating component of low energy ions to as low as L ~1.2 using observations from two polar-orbiting DMSP satellites at 840 km altitude. The ions observed at DMSP most often represent only the lowest energy bands seen at FAST altitudes because these are the energy bands with a precipitating component. The statistical study carried out by *Yao et al.* [2008] included both storm-time and quiet time ion bands, but the bands reported there did not extend to the low latitudes (~45°) or persist for as long as the storm-time bands reported here (although the lowest latitude bands reported in *Yao et al.* [2008] did coincide with the times of highest *AL*). A detailed examination of the storm-time energy-banded ions, including statistical and case studies, as well as an investigation into both the previously proposed generation mechanisms and other plausible mechanisms, are being presented in a separate paper (C. A. Colpitts et al., manuscript in preparation, 2013).

[5] Independent of these observations, *Parrot et al.* [2006a] reported the occurrence of banded emissions seen by DEMETER and associated with these same strong storms. The observation of these emissions during the same storms as the banded ions suggests a possible physical connection between the two phenomena, and leads us to investigate banded waves in the FAST data during these geomagnetic storms. Unlike the banded ions, which can last for tens of hours or more, often throughout an entire storm, the emissions reported by *Parrot et al.* [2006a] typically last for several minutes and are confined to the local density trough. Observations of a different type of banded VLF electromagnetic emission on both FAST and DEMETER during the very large storms, lasting several hours, most intense during times of enhanced density rather than in the trough, and coincident with observations of banded ions, are reported herein.

[6] The appearance of the banded ions and the associated wave activity raises questions about the changes in the geospace system that characterize large magnetic storms and the role that the waves play in major storm phenomena. In this study, we attempt to characterize the waves, the conditions under which they occur, and investigate one possible generation mechanism. In Section 2 a brief description is given of the instrumentation onboard the FAST and DEMETER satellites which provided the data for this study. Section 3 presents the observations from both satellites, with specific case studies from very strong geomagnetic storms. In Section 4 we discuss the results and investigate possible means for the generation of these banded emissions. Section 5 outlines our conclusions and potential future work in examining the nature of these waves.

2. Instrumentation

[7] The data presented in this study come from two low-altitude polar orbiting satellites, FAST and DEMETER. Both satellites carry a full complement of field and particle detectors. The FAST satellite, launched August 21, 1996 into an elliptical polar orbit with perigee 350 km and apogee 4175 km, traverses the auroral zone four times per orbit across a wide range of altitudes and local times. The spin period is ~5 s and the satellite is oriented in "cartwheel" mode, having its spin axis nearly perpendicular to the orbital plane. FAST data presented herein come from the electrostatic analyzers (ESAs), described in detail by *Carlson et al.* [2001], the TEAMS (Time-of-flight Energy Angle Mass Spectrograph) instrument [*Klumpar et al.*, 2001], the EFI (Electric Field Instrument) [*Ergun et al.*, 2001], and the magnetic field instrument [*Elphic et al.*, 2001]. The ESAs cover the energy range 0.004–32 keV for electrons and 0.003–24 keV for ions. The TEAMS instrument uses an ESA and an accelerating potential to separate ions into individual species (H^+, He+, He++, and O+) from 0 to 10 keV, and covers all polar angles. The electric field quantities are calculated from the voltage difference between pairs of spherical probes on three-axis dipole antennas, and the spectral coverage is from DC to ~4 MHz. The DC and AC magnetic fields are measured with three-axis fluxgate and search-coil magnetometers, covering frequencies from DC to ~500 kHz.

[8] The DEMETER satellite was launched on June 29, 2004 into a circular sun-synchronous polar orbit at an altitude of 710 km, with data recorded at all invariant latitudes less than ~65°. DEMETER data shown here are from the electric field instrument (described in further detail by *Berthelier et al.*, [2006a]), search coil magnetometer [*Parrot et al.*, 2006b], Langmuir probe [*Lebreton et al.*, 2006], and thermal ion spectrometer [*Berthelier et al.*, 2006b]. The electric field is obtained from voltage differences between four probes giving the three components covering the frequency range from DC to 3.3 MHz, although only one component in the VLF range is transmitted. The search coil magnetometer measures the three components of the magnetic field from a few Hz up to 20 kHz. The electron density and temperature are measured with the Langmuir probe, and the ion density, temperature, composition, and velocity are measured with the thermal ion spectrometer.

3. Data Presentation

[9] Figure 1 shows a typical example of banded ions observed during very strong (Dst <−100 nT) geomagnetic storms. In all panels the *x* axis represents time from 06:48–06:58 UT on November 8, 2004, with invariant latitude, magnetic local time, and altitude also indicated. This time corresponds to the main phase of the storm, ~2 h after onset, when Dst was ~−370 nT and solar wind speed was ~700 km/s. The top panel shows the energy flux of the downgoing ($150° < \theta < 210°$) ion population, from 10 to 10,000 eV, with the log of the energy flux in the color scale.

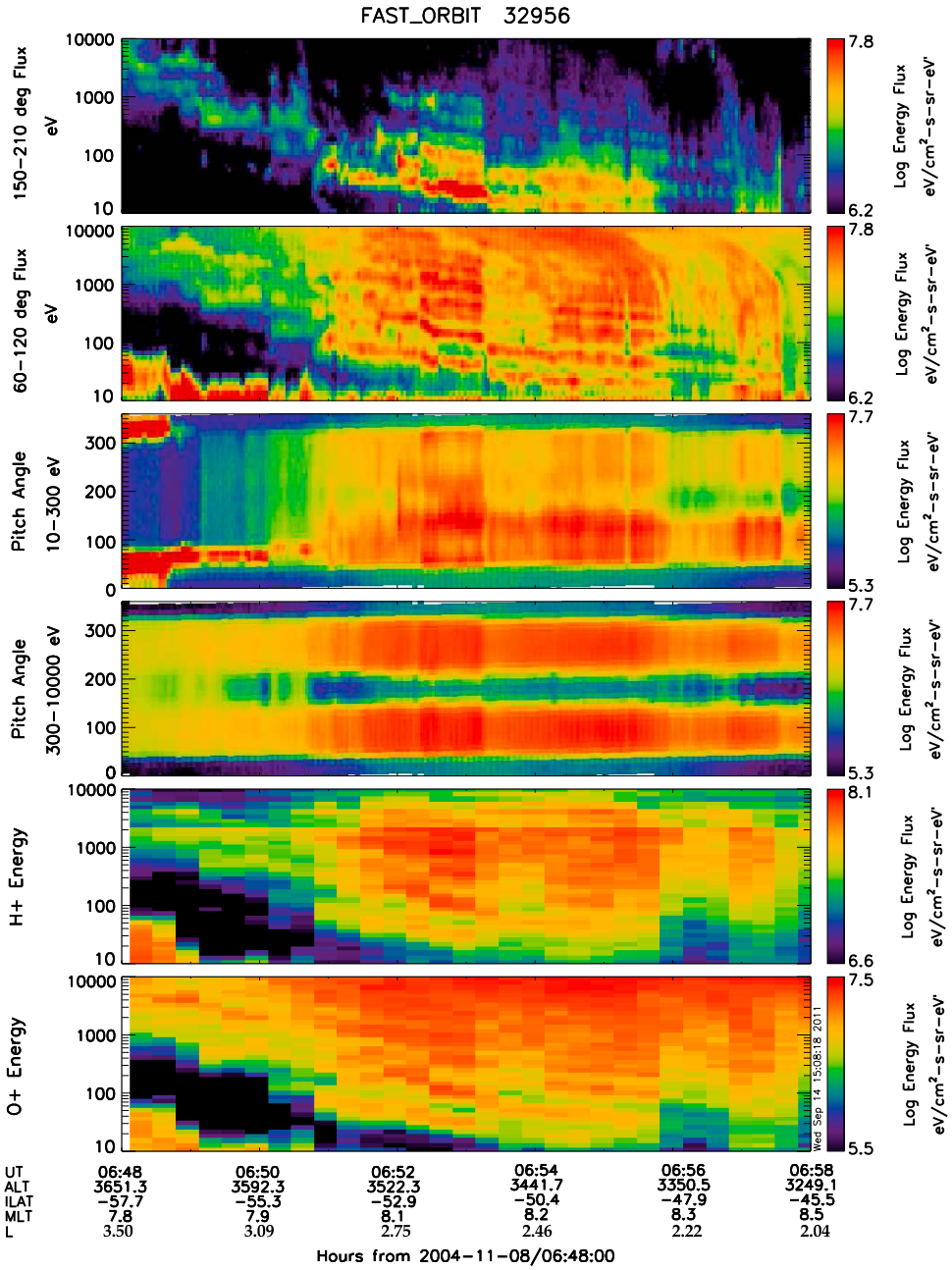

Figure 1. Banded ions observed during a strong geomagnetic storm from 06:48–06:58 UT on November 8, 2004, with time, altitude, invariant latitude, magnetic local time, and L-shell on the x axis. From top to bottom: energy flux of the downgoing ($150° < \theta < 210°$) ion population, from 10 to 10,000 eV, with the log of the energy flux in the color scale; perpendicular ($60° < \theta < 120°$) or trapped ion energy flux; 0–360 degree pitch angle distribution over the energy range 10–300 eV; 300–10,000 eV pitch angle distribution; energy flux (averaged over all pitch angles) of H^+ ions; and energy flux of O+ ions.

The second panel shows the perpendicular ($60° < \theta < 120°$) or trapped ion energy flux, with the same scales, and the third and fourth panels show the 0–360 degree pitch angle distributions over two different energy ranges, 10–300 eV and 300–10,000 eV, with the same color scale. These energy ranges were selected to illustrate specific features in the two populations as described below.

[10] Banded ions are visible in the top two panels as intense (red) fluxes, occurring in discrete bands at energies ~10–10,000 eV and lasting from ~6:48–6:58 UT (ILat ~−45.5 to −57.0; MLT ~7.9–8.5). They are distinct from the broadband dispersive ion injection events, reported by *McFadden et al.* [2001], which are visible in the second panel at high energies and low latitudes, though the bands seem to co-exist with the broadband injections in this region. The energy flux of the banded ions peaks in the perpendicular population (second panel), but is also observed in the lower energy bands in the precipitating ions (top panel). There is little or no upgoing component (not shown here) in the bands. This pitch angle distribution is shown in the third and fourth

Table 1. List of Major Geomagnetic Storms Investigated

Date	Min Dst	Banded Ions	Banded Waves
	FAST Waves		
05/03-05/07/98	−205	Y	Y
08/26-08/31/98	−155	Y	Y
09/25-09/26/98	−207	Y	Y
09/22-09/24/99	−173	Y	Y
10/22-10/25/99	−237	Y	Y
04/06-04/08/00	−288	Y	Y
07/15-07/17/00	−301	Y	P
08/12-08/14/00	−235	Y	P
09/17-09/19/00	−201	Y	Y
10/04-10/06/00	−182	Y	Y
11/06-11/07/00	−159	Y	Y
	DEMETER Waves		
07/26-07/30/04	−197	Y	Y
08/30-08/31/04	−126	Y	Y
11/07-11/12/04	−373	Y	Y
01/18-01/20/05	−121	Y	P
01/21-01/23/05	−105	Y	Y
05/08-05/10/05	−127	Y	P
05/15-05/19/05	−263	Y	Y
05/20-05/22/05	−103	Y	Y
05/30-05/31/05	−138	Y	Y
06/12-06/13/05	−106	Y	Y
08/24-08/26/05	−216	Y	Y
08/31-09/03/05	−131	Y	Y
09/11-09/12/05	−147	Y	Y
04/14-04/15/06	−111	Y	Y
12/15-12/16/06	−146	Y	Y

panels, with a clear double loss cone at the higher energies (fourth panel) and the downgoing loss cone largely filled in at lower energies (third panel). This is the typical pitch angle structure of the ion bands, although, in some cases, a significant upgoing ion component appears at low invariant latitudes. As is typical of these banded ion observations, the lower energy bands extend farther equatorward (to the right in Figure 1). The rise in energy at higher invariant latitudes, visible in this case, is often but not always observed. These bands were observed over several orbits at similar latitudes in both dawn and evening (not shown) sectors. The signature was more pronounced in the dawn sector, as is typically observed. In this event the banded ions lasted ∼10 h. Similar banded ions, lasting in some cases up to 12 h, are observed in every very large (Dst <−150 nT) geomagnetic storm observed with the FAST satellite (launched August 1996), but no Dst <−150 nT events occurred before May 1998 or after August 2005. Between those times a total of 26 storms with Dst <−150 nT occurred, 15 during times when either FAST or DEMETER carried out wave observations. Because DEMETER was operational during a less active time period, Dst <−100 nT events were also considered, adding another 10 events to the study, all of which included banded wave observations. See Table 1 for storm details.

[11] The bottom two panels of Figure 1 show the energy flux of H^+ and O+ ions, using the TEAMS ion mass spectrometer data. Note that the color scales are different in each panel. Ion bands are observed in both species, which is not uncommon. There are several bands visible at the same energies in both species, particularly the lower energy bands (∼20–300 eV) as well as some higher energy bands. The design of the TEAMS instrument coupled with the large difference in mass/charge ratio of these species (including the He+ ions shown in Figure 6) ensures that there is not significant cross-talk between the channels and that the presence of these bands in multiple species is physical rather than instrumental [*Klumpar et al.*, 2001]. The two widely accepted means for generation of ion bands, time-of-flight dispersion and convective drift dispersion, both result in banding of different species at the same velocity, and therefore different energies. The ion bands observed here during superstorms represent a new phenomenon that requires a new explanation, and examination of the concurrent banded waves could provide insight into these banded ions.

[12] The wave electric field data needed to examine these banded emissions are only available on FAST through January 2001, and therefore are not available for the interval in Figure 1. For strong storms after January 2001, it is useful to look at wave data from other satellites that cover similar L-shells, altitudes and local times as FAST, in conjunction with the FAST ion data. Figure 2 shows data from the DEMETER satellite during the same storm for which FAST ion data were shown in Figure 1, from 06:24:30–07:02:30 on November 08, 2004, with MLT and geomagnetic latitude and longitude included for reference. This is the same half-orbit plotted in Figure 1 of *Parrot et al.* [2006a], and the top three panels are quantities also plotted in that figure. The top two panels of Figure 2 show 0–1500 Hz spectrograms of one component of the electric and magnetic fields. The electric field component is perpendicular to the orbital plane.

[13] Several emissions are visible in these spectrograms which are not the focus of this study, most notably the intense "bursty" emissions at ∼650–1250 Hz from ∼6:54–6:57 which were the focus of *Parrot et al.* [2006a]. We focus on the banded emissions, evident in both the electric and magnetic field during two intervals, ∼06:29–06:43 and ∼06:45–06:55, that appear as discrete frequency bands between ∼120 and ∼650 Hz separated by ∼100 Hz. These banded emissions persist for several DEMETER orbits, lasting ∼8 h, in both the northern and southern hemispheres.

[14] Table 1 lists all of the storms investigated for this study, along with the minimum Dst and a summary of the observations for each storm. Banded ions are observed on FAST during every large geomagnetic storm investigated, and banded waves are observed during all storms for which there are DEMETER data. A statistical study of DEMETER banded wave observations was performed, and the waves were observed on 45 orbits during 15 separate strong storms from 2004 to 2006 (see Table 1). This study also included quiet time observations, with 600 randomly selected orbits during extended quiet times (>1000 h. of Dst continually >−50 nT). Within these quiet time observations there was some evidence of similar banding waves, but these quiet time bands lasted only for minutes (in contrast to the several hour duration of the storm time bands), were 1–2 orders of magnitude weaker than the storm time bands, and were not evident in the wave magnetic field data. Banded ions on FAST during these quiet time observations, when there was data available, were either not present or much less intense than the storm time ion bands. The storm time banded waves can be observed during either the main phase or the recovery phase of the storms, and in some storms they are observed throughout both phases. In some cases (indicated by a 'P' in Table 1) there is evidence of wave banding but the waves

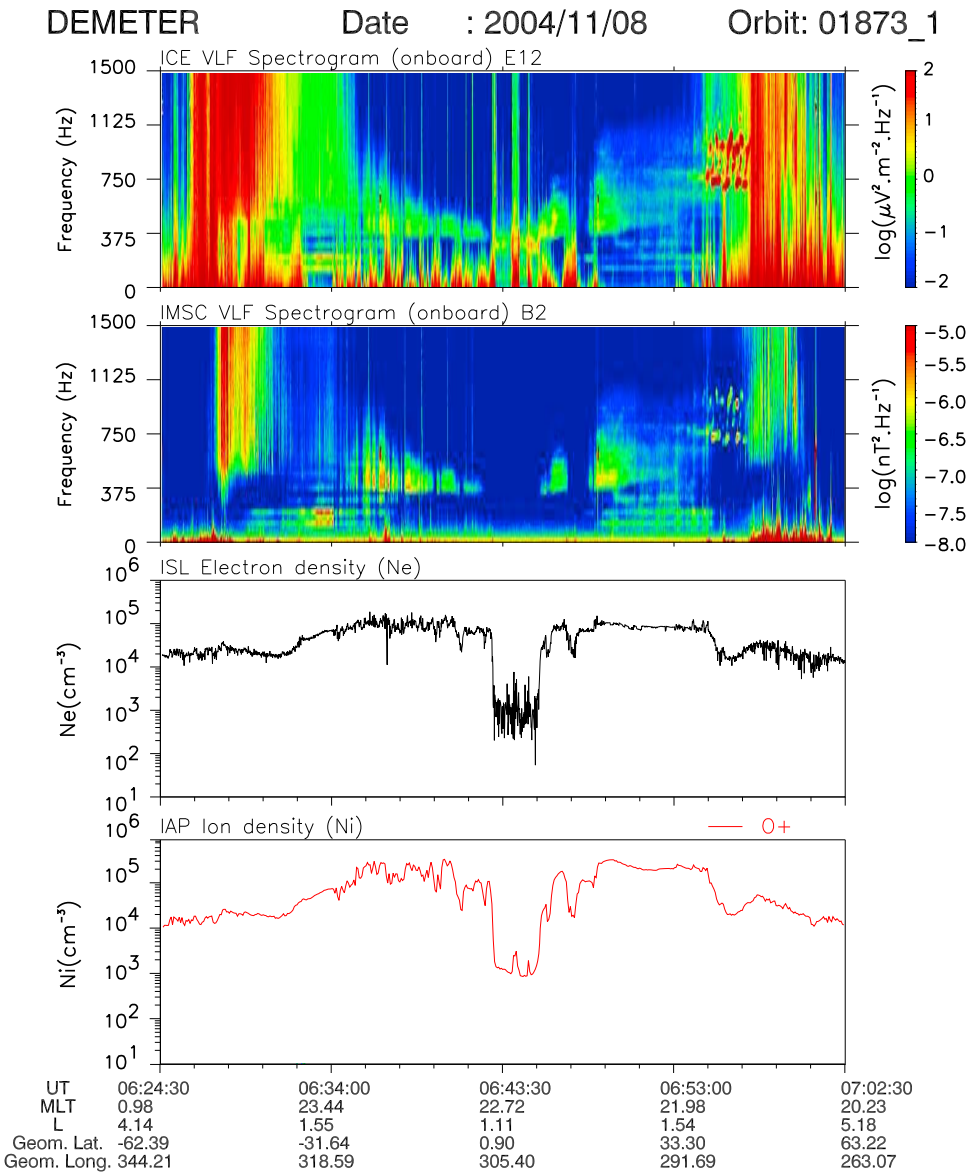

Figure 2. DEMETER satellite data from 06:24:30–07:02:30 on November 08, 2004, with UT, MLT and geomagnetic latitude and longitude on the *x* axis. From top to bottom: 0–1500 Hz spectrogram of the component of the electric field perpendicular to the orbital plane; 0–1500 Hz spectrogram of one component of the magnetic field; electron density; and ion density separated into its components: O+ (red, the dominant component in this region), He+ and H^+ (near noise level, not shown).

do not share all of the characteristics of the emissions reported here. Specifically in these cases there was either only one visible frequency band or the bands were observed intermittently.

[15] In addition to characterizing the waves of interest, the data in Figure 2 allow us to examine the plasma conditions in which the waves are observed. The bottom two panels of Figure 2 show the electron and ion densities measured with the ISL (Langmuir probe) and IAP (thermal ion spectrometer) instruments, with the ion density separated into its components: O+, the dominant component in this region, is the only species shown; He+ and H^+ are near the noise level and not shown. The banded emissions appear to correlate with enhancements in both the electron and warm ion densities. To investigate the relationship between density and observations of the banded emissions, Figure 3 shows 0–1500 Hz spectrograms of a time period selected from Figure 2, 06:29:00–06:42:30, along with the ion and electron densities. The banded emissions correlate fairly well with enhancements in both electron and warm ion density, and closer examination indicates that they follow the observed warm ion density more closely. In particular, several brief periods of increased intensity of the waves from ~06:35–06:39 coincide with increases in warm ion density that are not apparent in the electron density. Given that quasi-neutrality requires that the total electron and ion densities are roughly equal, the differences are most likely due to the different energy ranges covered or other instrumental effects.

[16] The DEMETER satellite included a burst mode, providing for higher time resolution electric and magnetic field

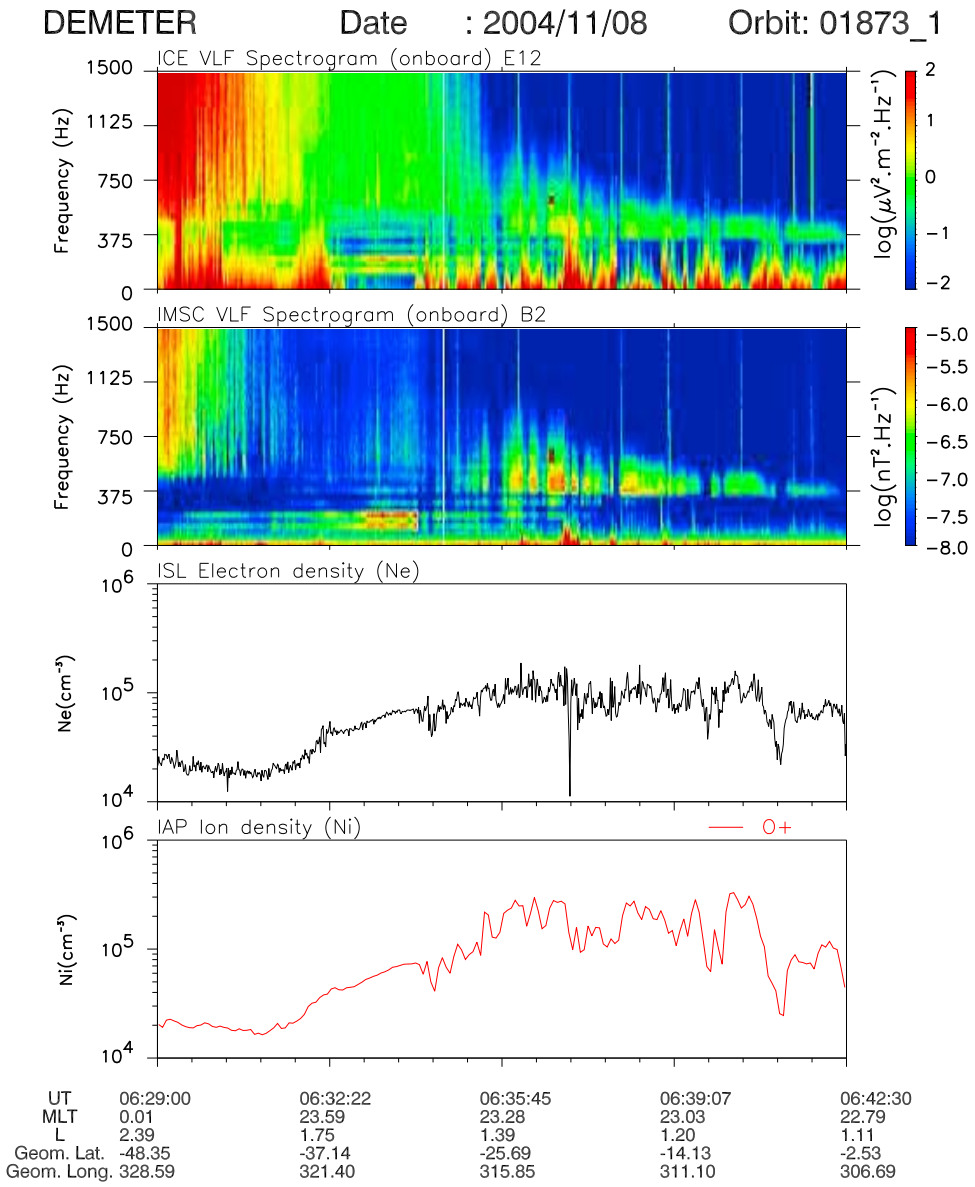

Figure 3. Expanded 0–1500 Hz spectrograms of a time period selected from Figure 2, 06:29:00–06:42:30, along with the ion and electron densities. The banded emissions correlate well with enhancements in the density.

waveforms and allowing for a closer examination of the observed density correlation. As the burst mode was not generally triggered by VLF wave activity, there are relatively few bursts during the times of banded wave observations. Figure 4 shows one such interval, from 03:17:30–03:19:00 on November 8, 2004, during the same storm as the previous two figures but two orbits earlier. The banded emissions are visible in both the electric and magnetic field, ranging from ~150–650 Hz and separated by ~100 Hz. The E/B ratio of the waves is $\sim 10^5$ m/s, consistent with electromagnetic emissions. The burst data show a clear correlation between the waves and enhancements in both the warm ion and electron densities. There are no DEMETER DC magnetometer data available from the exact times of Figures 2, 3, and 4, but calculations using a model magnetic field, as well as data from adjacent orbits when the spacecraft is in the same location, give a proton cyclotron frequency of f_{cp} = ~350–550 Hz in this region. Thus, the frequency separation Δf is much less than the local cyclotron frequency, and if the waves are generated at harmonics of f_{cp} their source region must be at considerably higher altitudes (~5000 km for f_{cp} = $\Delta f \sim 100$ Hz). These waves would then propagate to the DEMETER spacecraft location, as described below. As discussed by *Pfaff et al.* [2008], scattering due to plasma irregularities associated with density depletions could explain why the waves are less intense in the regions of lower density.

[17] For storms when there are FAST AC electric field data, we observe banded wave emissions at the same location as the banded ions. Figure 5 shows an example of simultaneous FAST observations of banded ions and banded VLF wave emissions from 05:06–05:08 on August 30, 1998

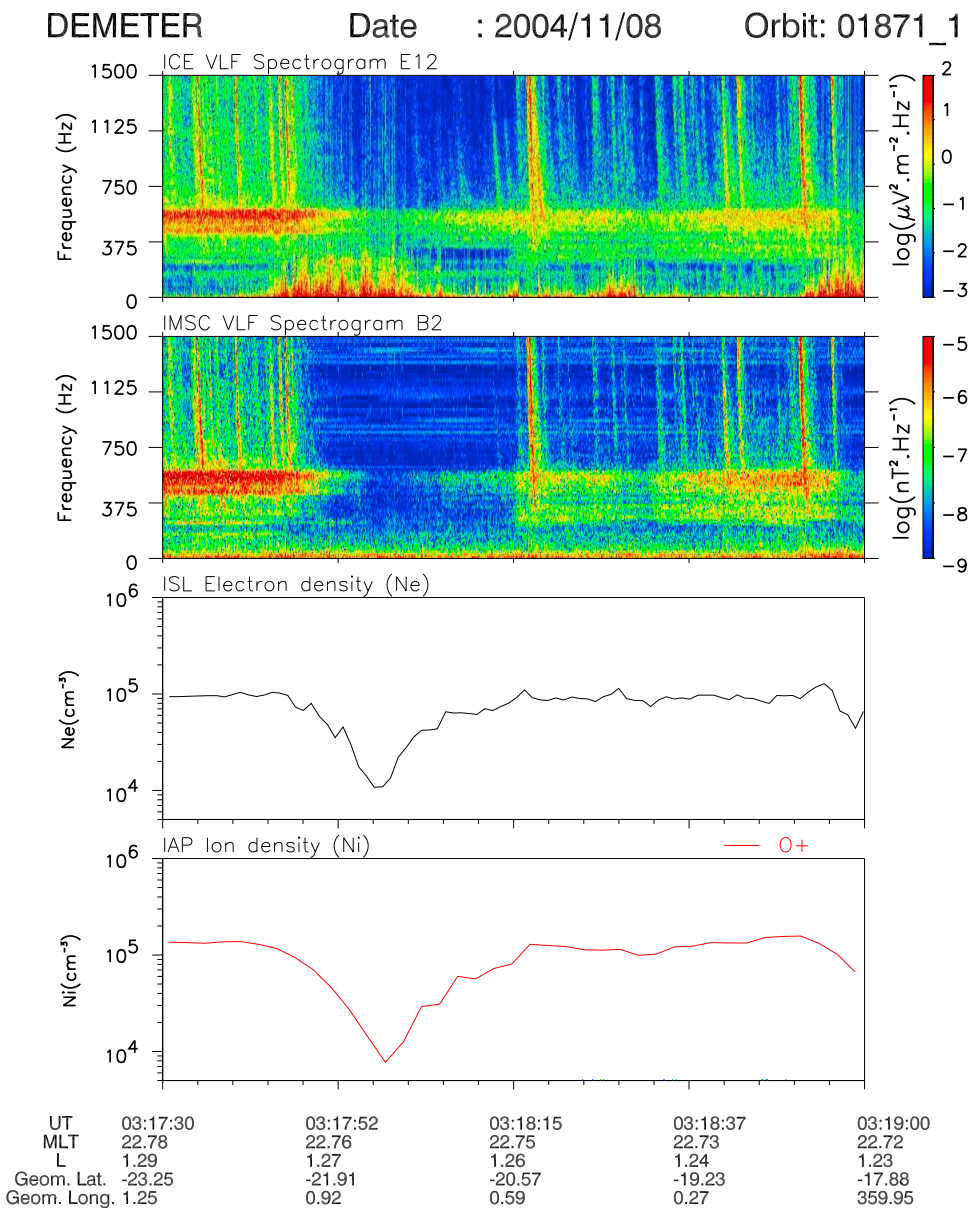

Figure 4. DEMETER burst data from 03:17:30–03:19:00 on November 8, 2004, providing for higher time resolution electric and magnetic field waveforms. From top to bottom: 0–1500 Hz spectrogram of the component of the electric field perpendicular to the orbital plane; 0–1500 Hz spectrogram of one component of the magnetic field; electron density; and ion density separated into its components: O+ (red, the dominant component in this region), He+ and H^+ (near noise level, not shown).

(during the recovery phase of the storm, ~3 days after the peak Dst of −155 nT, with Dst ~−50 nT and solar wind speed ~570 km/s). The top panel shows the "omni-directional" (spin plane only) wave electric field power computed onboard with the DSP (digital signal processor), over the frequency range 0–2.5 kHz. The second panel shows the ion energy flux (averaged over all pitch angles). Banded ions are observed throughout this time period at energies from ~200 eV to 10 keV. Banded waves at frequencies ~700–2000 Hz, appearing as discrete frequency bands separated by ~200 Hz, are also observed during periods within this interval, most notably ~05:07:15–05:07:40 and ~05:08:20–05:09:00, when the banded ions are most intense. Similar waves are observed during the times of the banded ion observations in every storm for which the FAST satellite transmitted AC electric field data (Table 1). As was the case for DEMETER observations, during some storms ('P' in Table 1) the banded waves observed by FAST don't share all of the characteristics of the emissions reported here. In these cases the waves either didn't last long enough to get a clear determination of their structure or the bands did not remain at constant frequency.

[18] The third panel of Figure 5 shows the ion pitch angle distribution for energies from 4 to 30,000 eV. Unlike in the example shown in Figure 1, the downgoing loss cone is completely filled in, and in this case the downgoing and perpendicular ion energy flux is approximately the same, with bands at the same energies in both populations.

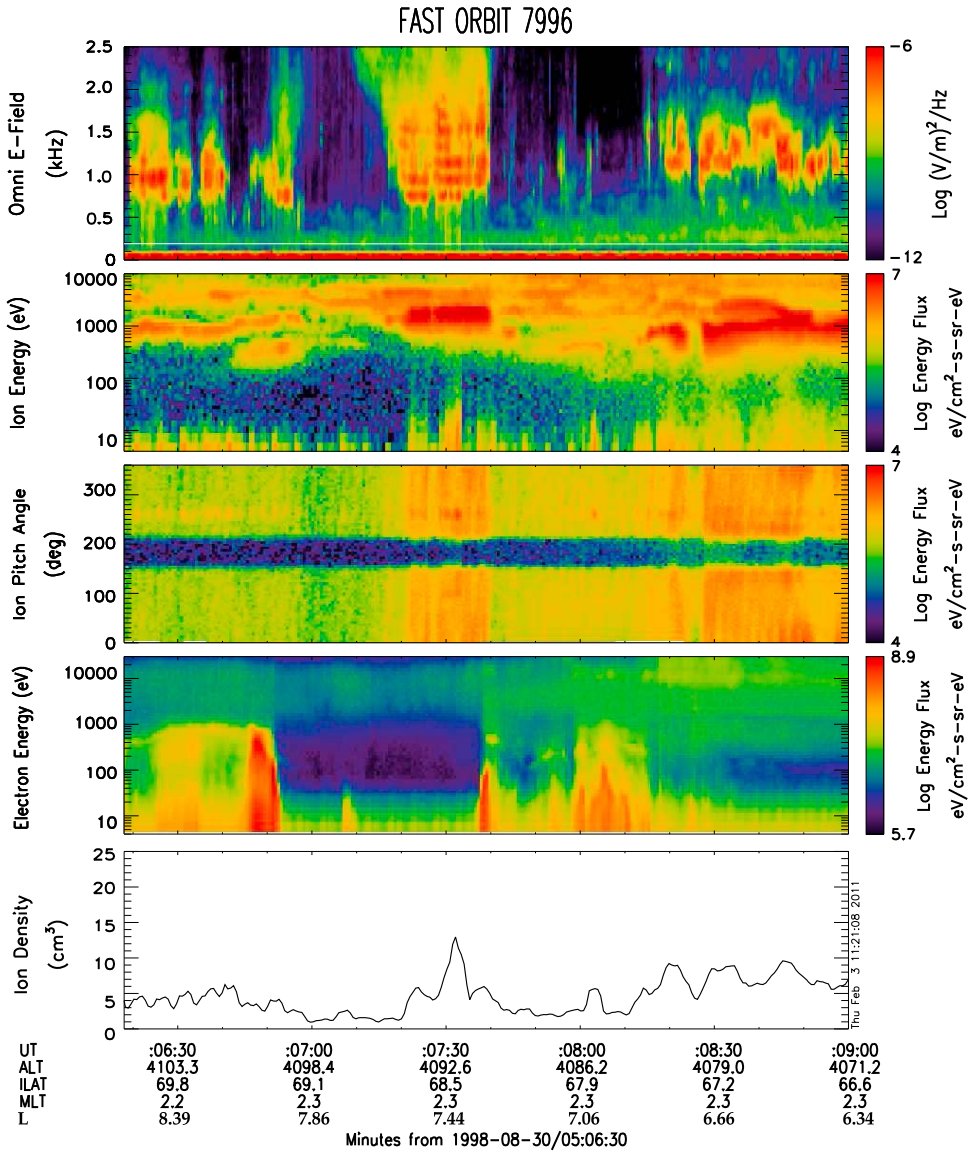

Figure 5. Simultaneous FAST observations of banded ions and banded VLF wave emissions from 05:06:15–05:09:00 on August 30, 1998. From top to bottom: omni-directional wave electric field power computed onboard with the DSP (digital signal processor), over the frequency range 0–2.5 kHz; ion energy flux (averaged over all pitch angles); ion pitch angle distribution for energies from 4 to 10,000 eV; 4–30,000 eV electron energy flux (averaged over all pitch angles); and ion density, approximated by integrating the particle flux over the energy range 4–30,000 eV, and averaged over every 2.0 s to eliminate large fluctuations.

The fourth panel shows the 4–30,000 eV electron energy flux (averaged over all pitch angles). The bottom panel shows the warm ion density, approximated by integrating the ion flux over the energy range 4–30,000 eV, and averaged over every 2.0 s to eliminate large fluctuations. The banded waves occur during warm ion density enhancements, visible in both the increased intensity of the ion bands in the second panel and increases in ion density in the bottom panel, during the times of the banded wave emissions. This is consistent with the enhanced ion density during the DEMETER observations, which can be seen in the calculated ion density (Figures 2, 3, and 4 (bottom)), though there is no instrument on DEMETER with which to see possible energy bands in the ions. The banded waves also appear anti-correlated with large fluxes of broadband (4–1000 eV) electrons. The magnetic field data (not shown) indicate field-aligned currents (FAC) during the times of the strong broadband electron events, with little or no FAC during the times of the wave observations.

[19] Figure 6 shows the energy flux from 4 to 10,000 eV, averaged over all pitch angles, of three ion species from the TEAMS instrument during the same time period as Figure 5. The top panel is the total ion energy flux, and the bottom three panels are the H^+, O+, and He+ energy flux respectively. As in the case shown in Figure 1, several energy bands are visible in the H^+, O^+, and He^+ populations at the

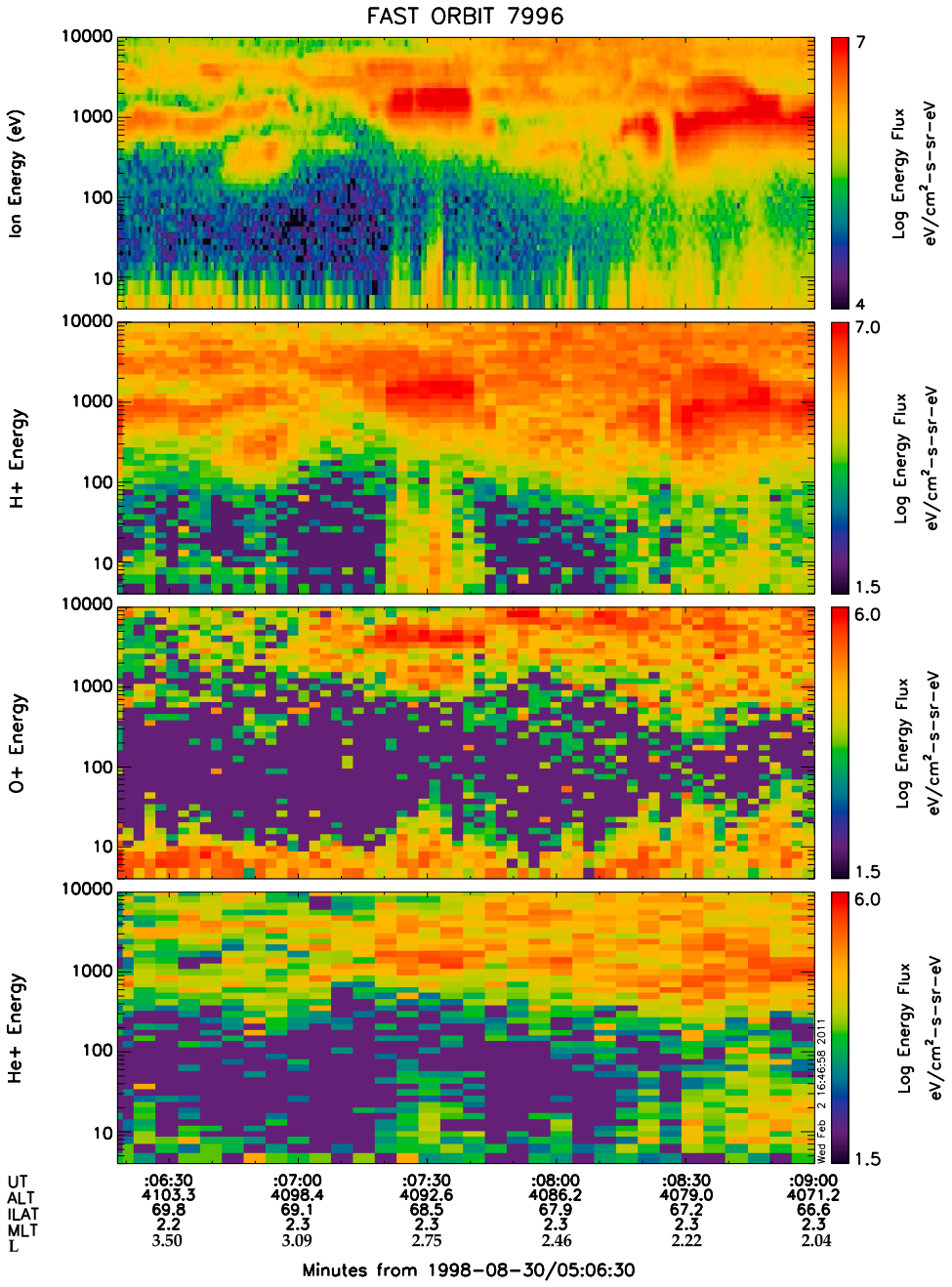

Figure 6. The 4–10,000 eV energy flux of three ion species from the TEAMS instrument during the same time period as Figure 5, averaged over all pitch angles: total ion energy flux (first panel) and H^+, O+, and He+ energy flux (second, third, and fourth panels).

same energies (in particular ~2000 and ~5000 eV from 05:07:15–05:07:45), ruling out time of flight mechanisms for the generation of the bands.

[20] An expanded view of the interval from 05:07:05–05:07:45 is shown in Figure 7. The top panel shows the 0–3 kHz wave spectrogram, with the local proton gyrofrequency (f_{cp} ~195 Hz), the 4th and 5th harmonics of f_{cp}, and the lower hybrid frequency ($f_{lh} = [(f_{ci}*f_{ce})^{-1} + f_{pi}^{-2}]^{-1/2}$, calculated from the ion density shown in Figure 5 and the proton gyrofrequency) overplotted. The calculated lower hybrid frequency includes the integrated ion flux as a proxy for the density, and is unlikely to vary as much as indicated in the plot over this time, but is included to show that it is on the order of the frequency of the lowest observed bands. The lower panel shows the total ion energy flux (averaged over all pitch angles). The banded waves are very close to multiples of the proton gyrofrequency, without the fundamental and lowest harmonics, the lowest band is at ~$4f_{cp}$, close to f_{lh}.

[21] Figure 8 (top) shows a single line spectra at 05:07:29, with electric field power as a function of frequency. Several individual bands are evident, and the amplitudes of the bands relative to each other and to the background can be seen. The spacing between the peak amplitudes of the bands during this

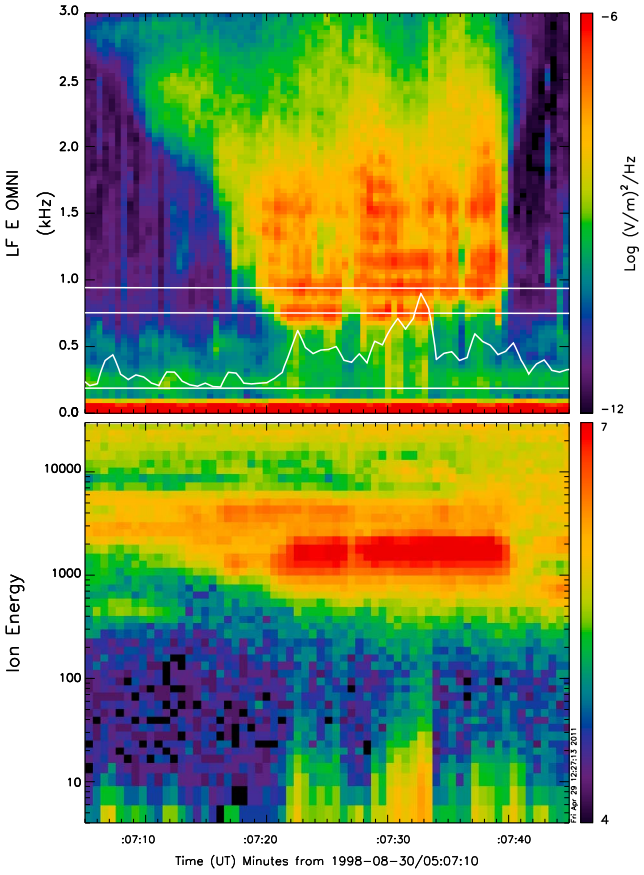

Figure 7. Expanded view of the interval from 05:07:05–05:07:45. (top) The 0–3 kHz wave spectrogram, with the local proton gyrofrequency (f_{cp} ~195 Hz), the 4th and 5th harmonics of f_{cp}, and the lower hybrid frequency (calculated from the ion density shown in Figure 5 and the proton gyrofrequency) overplotted. (bottom) Total ion energy flux (averaged over all pitch angles).

time was found to be ~185 Hz, slightly lower than the local proton gyrofrequency (~195 Hz), and therefore equal to the proton gyrofrequency at a slightly higher altitude. The 4th and 5th harmonics of f_{cp} are overplotted, f_{lh} at this time is ~500 Hz (not shown). Figure 8 (bottom) shows a similar line plot generated from the magnetic field spectrogram of the same time period (B-field spectrogram not shown as strong spin tones mask the banded waves in the spectrogram). The banded waves are also evident in the magnetic field, indicating a magnetic component to the observed emissions. The magnetic component is comparable to that observed in the DEMETER emissions, with both yielding values of (E/B) ~ 10^5 m/s, consistent with electromagnetic emissions.

[22] FAST also included a burst mode, which provided 3-D electric and magnetic field measurements, enabling investigation of the polarization of the banded waves by looking at the electric field power both parallel and perpendicular to the earth's magnetic field. Figure 9 shows banded waves observed in the FAST burst data during the same storm as Figures 5–8 (08-30-1998), but one orbit earlier, from 02:53:30–02:55:00. The banded waves were observed throughout this storm, and the orbits shown in Figures 5–9 are representative orbits showing a clear example of banded waves as well as an example of burst data from 3 h earlier. The 4–30,000 eV ion energy flux (averaged over all pitch angles) is shown in the top panel. The lower three panels show the omni-directional electric field power, the component of the electric field power parallel to the ambient magnetic field, and the perpendicular component. The banded waves, evident in both the parallel and perpendicular components, again peak when the banded ions are most intense. There is more power in the perpendicular component, but there is a significant amount of power in the parallel component, suggesting that these waves are polarized obliquely to the geomagnetic field. Additionally, the lower frequency bands are more intense in the perpendicular component, and

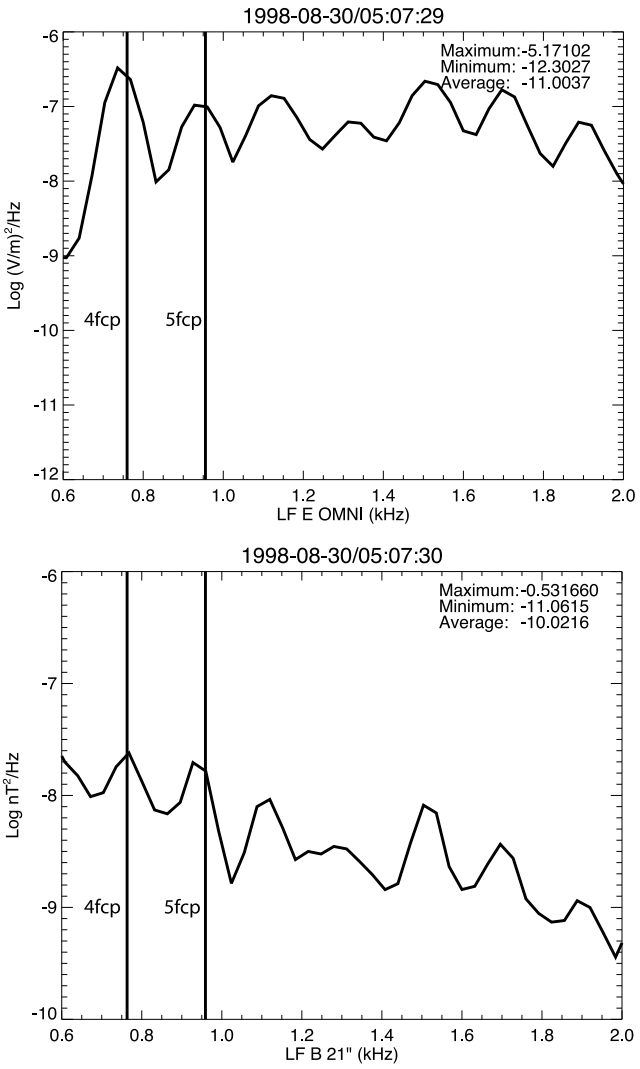

Figure 8. Single line spectra from 05:07:29. (top) Electric field power as a function of frequency. (bottom) Magnetic field power as a function of frequency. Several individual bands are evident in both E and B. The spacing between the peak amplitudes of the bands during this time was found to be ~185 Hz, slightly lower than the local proton gyrofrequency (~195 Hz), and therefore equal to the proton gyrofrequency at a slightly higher altitude. The 4th and 5th harmonics of the local f_{cp} are overplotted, f_{lh} at this time is ~500 Hz (not shown).

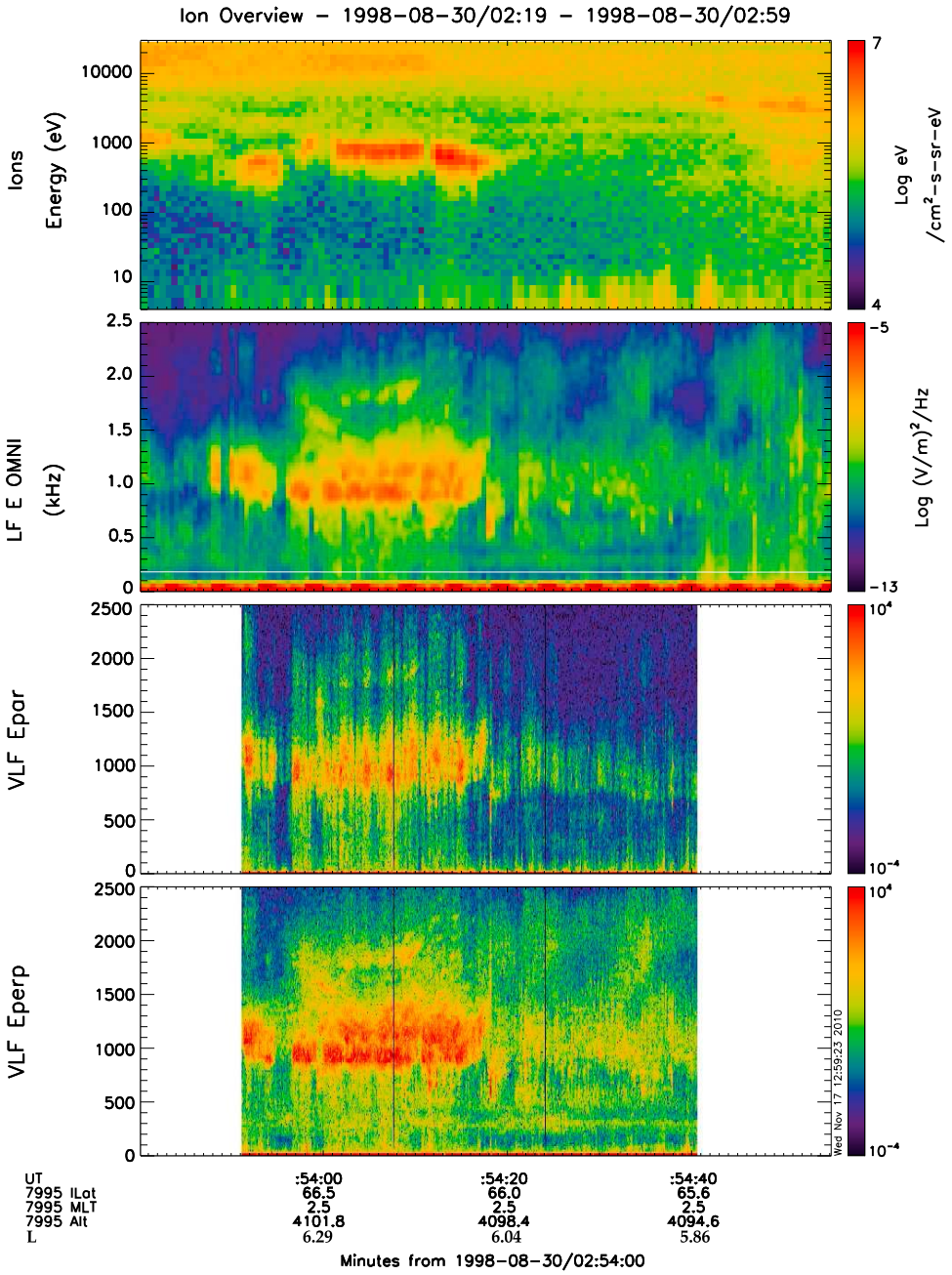

Figure 9. FAST burst mode data from 02:53:30–02:55:00 on 08-30-1998. From top to bottom: 4–30,000 eV ion energy flux (averaged over all pitch angles), omni-directional electric field power, the component of the electric field power parallel to the ambient magnetic field, and the perpendicular component of the electric field power.

extend into the region of less intense, higher energy ion bands (02:54:20–02:54:40).

[23] These banded emissions are observed over several orbits in every strong storm encountered by the FAST satellite. Figure 10 shows ion and wave data during four separate FAST passes through the southern hemisphere auroral zone on 05 May 1998. The top panels show the ion energy flux, integrated over all pitch angles, and the bottom panels show the omni-directional wave electric field power. In each pass, banded ions are visible in the top panels at energies 100–10,000 eV, and banded waves in the frequency range 0.2–1.6 kHz are evident in the bottom panels. As in the previous cases shown, the intensity of the banded emissions peaks when the banded ions are strongest, and the spacing between the banded waves (~150–200 Hz) suggests harmonic emissions, again with the lowest harmonics often not present.

[24] The banded emissions in Figure 10 are not as constant in frequency as, e.g., those shown in Figures 2, 3 and 7, and there are also fewer visible bands in Figure 10. The banded ions in Figure 10 are slightly less intense than the strong band visible in Figure 7, and tend to decrease in energy with

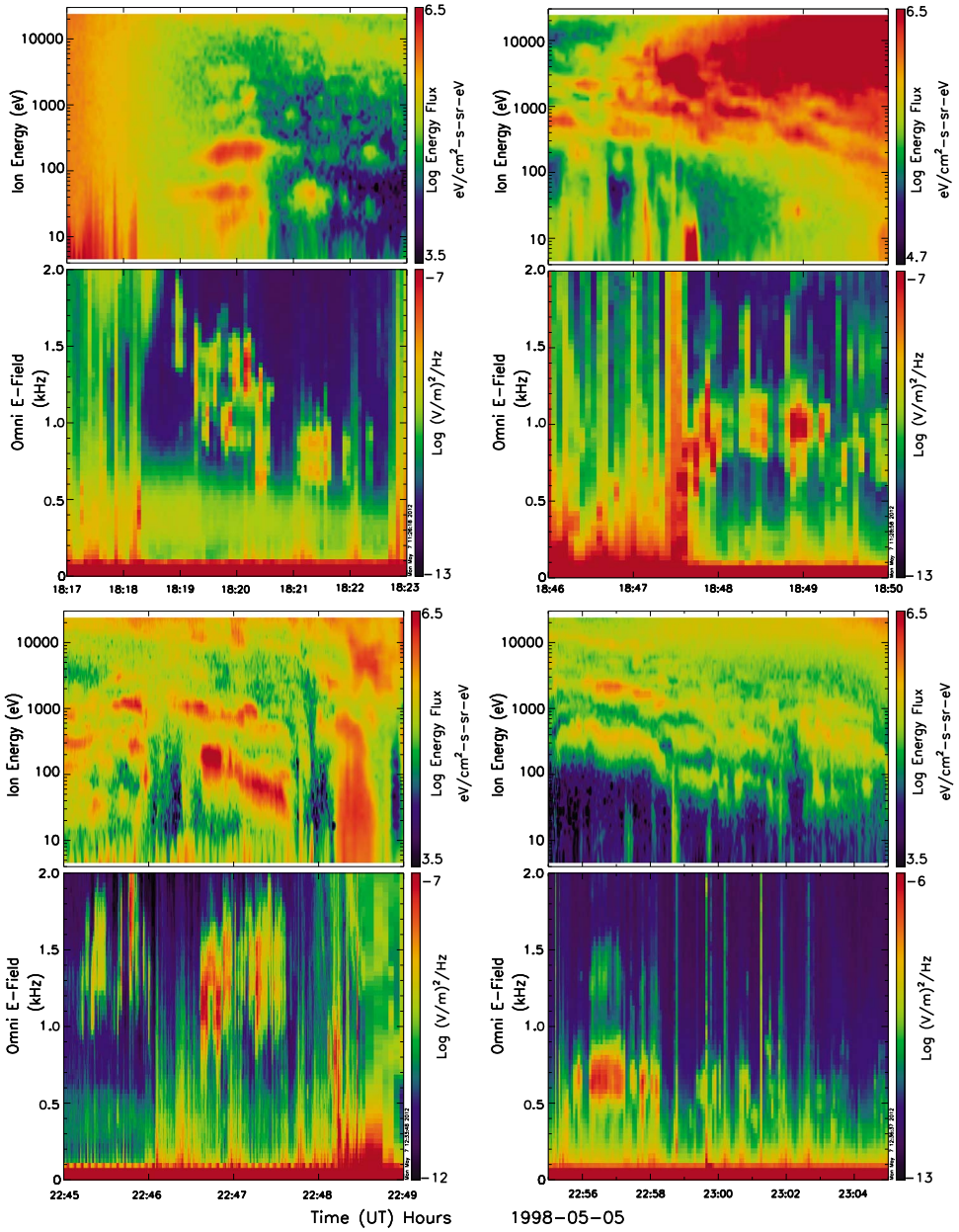

Figure 10. Ion and wave spectrograms from four FAST auroral passes on 05-05-1998, each with the ion energy flux, integrated over all pitch angles, in the top panel and the omni-directional wave electric field power in the bottom panel: (top left) 18:17:00–18:23:00 UT, (top right) 18:46:00–18:50–00 UT, (bottom left) 22:45:00–22:49:00 UT, and (bottom right) 22:55:00–22:05:00 UT.

decreasing latitude, similar to those in Figure 1. The lower intensity and changing energy of the ion bands may be associated with the changing frequency and fewer bands evident in the waves shown in Figure 10. Like the previous cases, the waves appear anti-correlated with large broadband electron fluxes (not shown), with the banded ions and waves appearing equatorward of the auroral electrons. Also as with the previous examples, the waves in Figure 10 have a significant magnetic component (E/B $\sim 10^5$, consistent with electromagnetic emissions) when the magnetic field data is available.

[25] Figure 11 shows ion and electric field spectrograms from 6 orbits during a separate storm, on 13 August 2000. The panels are the same as in Figure 10, and each pair of panels again represents one southern hemisphere auroral FAST pass. As in Figure 10, banded ions (top panels, in the energy range 20–20,000 eV) and banded waves (bottom panels, frequency 0.3–2.3 kHz) are evident on each orbit. Again the spacing between the banded waves suggests harmonic emissions, the waves occur equatorward of the auroral electrons (not shown), and there is a significant magnetic component when available (also not shown).

[26] Figure 12 shows data from an expanded time during the last orbit shown in Figure 11, with ion and electron energy flux in the top two panels (integrated over all pitch angles), omni-directional electric field power in the third, and

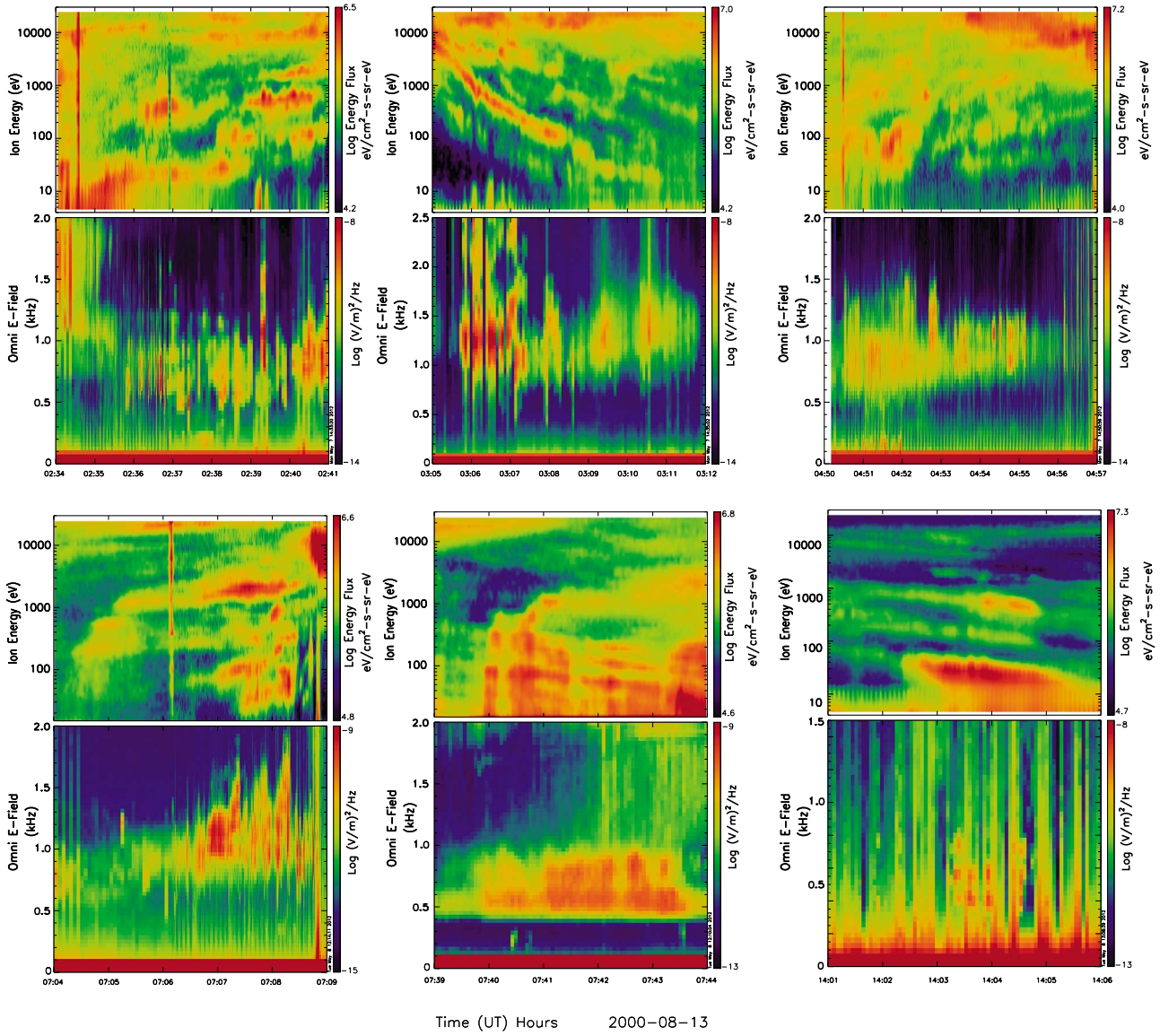

Figure 11. Ion and wave spectrograms from four FAST auroral passes on 08-13-2000, each with the ion energy flux, integrated over all pitch angles, in the top panel and the omni-directional wave electric field power in the bottom panel: (top left) 02:34:00–02:41:00 UT, (top middle) 03:05:00–03:12–00 UT, (top right) 04:50:00–04:57:00 UT, (bottom left) 07:04:00–07:09:00 UT, (bottom middle) 07:39:00–07:44:00 UT, and (bottom right) 14:01:00–14:06:00 UT.

magnetic field power in one perpendicular direction in the bottom panel. The broadband auroral electrons are visible from ~07:30–07:37 UT, and the banded waves are evident in both the electric and magnetic field from 07:38–07:46. This anti-correlation of the banded emissions with the electrons and significant magnetic component are seen throughout all the geomagnetic storms.

[27] The ion (and wave) bands in Figures 10–12 are not as constant in energy (frequency) as those shown, e.g., in Figure 7, and tend to be slightly less intense. However, these two figures show that the banded ions and waves persist over several hours throughout major geomagnetic storms. The presence of the banded emissions coincident with the most intense banded ions, equatorward of the auroral electrons, and throughout the storms provides evidence that the waves are associated with these storm-time banded ions, which will be investigated further in the next section.

4. Discussion

[28] The coincidence of the frequency-banded wave emissions with energy-banded ions during very large geomagnetic storms suggests that the ions may play a role in the generation of the banded waves. Specifically, the free energy in the ion distribution, arising from the positive slope in the ion velocity due to the bands, can give rise to wave growth at certain resonant frequencies. *André et al.* [1986] observed wave emissions at harmonics of the ion gyrofrequency with the S3–3 satellite and confirmed the observed wave growth theoretically with a positive slope in a model ion distribution.

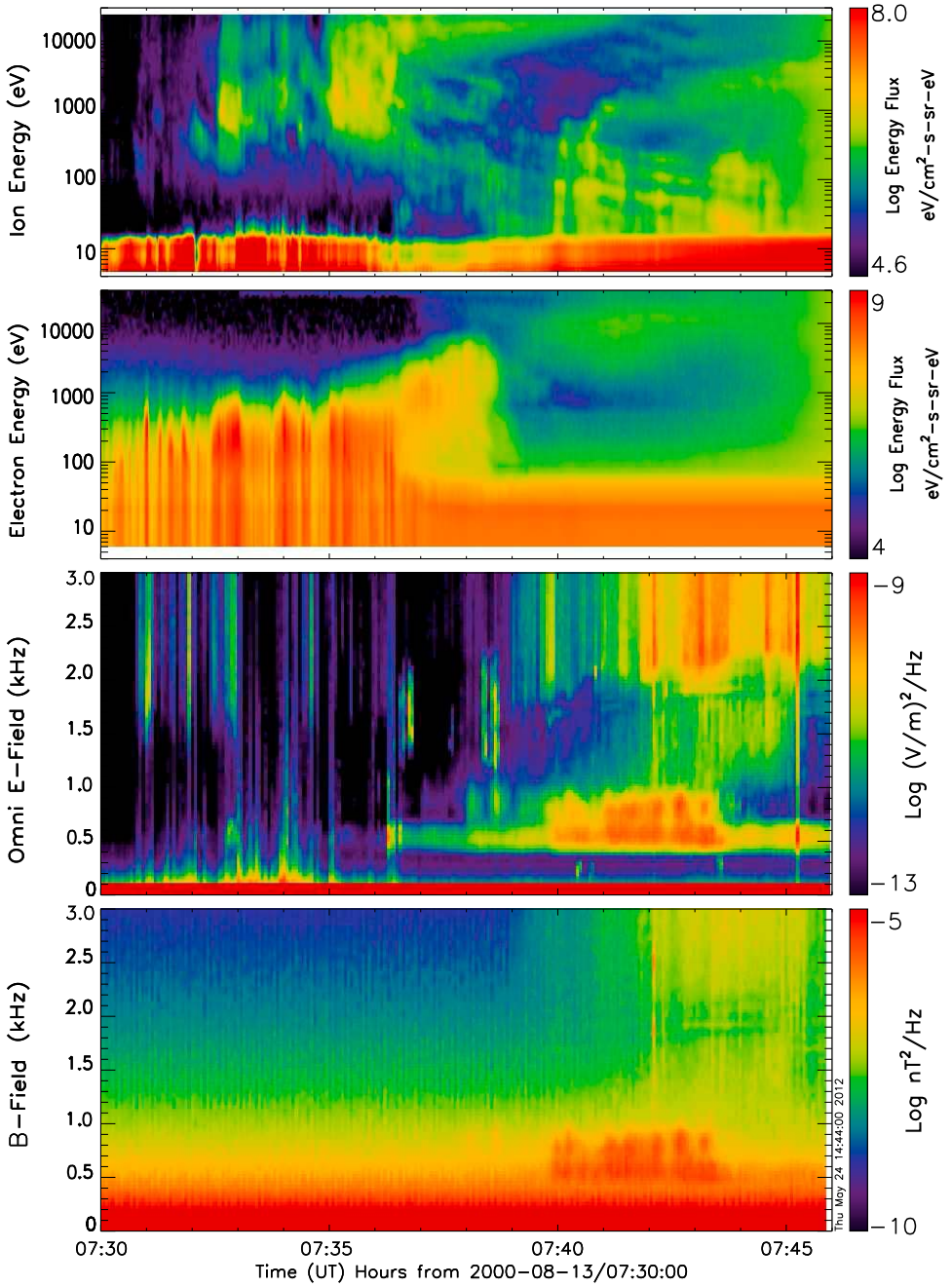

Figure 12. Ion, electron, electric field, and magnetic field data from an expanded time of the last FAST orbit shown in Figure 11, 07:30–07:56 UT on 13 August 2000. From top to bottom: ion energy flux, integrated over all pitch angles; electron energy flux, integrated over all pitch angles; omni-directional wave electric field power; and magnetic field power along one perpendicular direction.

Cattell and Hudson [1982] observed lower hybrid waves and ion gyroharmonics near the lower hybrid frequency, also with S3–3, and found that wave growth at these frequencies resulted from coupling of the lower hybrid and ion Bernstein instabilities using a model ion ring distribution. *Roth et al.* [1983] reported wave observations at gyroharmonics near the lower hybrid frequency resulting from an artificially injected plasma beam as part of the Porcupine sounding rocket experiment, also invoking a combination of the lower hybrid instability and resonant particle interaction at ion gyroharmonics to theoretically generate the observed emissions. *Roth and Hudson* [1985] further separated the wave-particle interaction exciting these waves (observed on both S3–3 and DE) into linear growth, trapping, and nonlinear diffusion, and found that the resulting waves play an important role in heating heavier ions and energizing ion conics in the cusp. To explore the possible generation of the waves reported here, we first consider the ion gyrofrequency at the location of the observed waves relative to the frequency of the wave bands to see if the emissions could be locally generated at these frequencies, and then employ a linear

Table 2. WHAMP Particle Input Parameters

One Ring, H^+ Only		
Species	Density (cm-3)	Temp (keV)
H^+	10	0.9
H^+	−8	0.15
e−	2	0.02
Two Rings, H^+ Only		
Species	Density	Temp
H^+	10	0.9
H^+	−3.5	0.15
H^+	3	4
H^+	−7.5	2
e−	2	0.02
One Ring, H^+ and O+		
Species	Density	Temp
H^+	10	0.9
H^+	−8	0.15
O+	10	0.9
O+	−8	0.15
e−	4	0.02

dispersion relation solver to investigate wave growth at specific frequencies.

[29] For the storms with FAST wave data, such as the example in Figures 5–9, we can compare the frequency spacings between bands directly with the local ion cyclotron frequency. As shown in Figure 7, the proton cyclotron frequency during the times of the wave observations was ∼195 Hz, and from Figure 8 the spacing between bands was determined to be ∼185 Hz. If the waves were generated at harmonics of the proton gyrofrequency, such that $\Delta f = f_{cp}$, at a slightly higher altitude than that of the FAST satellite at this time (∼4000 km), the resulting frequency structure would match that observed.

[30] For the DEMETER satellite observations (at ∼710 km altitude), the statistical study of banded waves observed on 36 orbits during 14 separate strong storms that was carried out also included calculations of the local gyrofrequency. The local proton gyrofrequency at this altitude is much higher (∼300–600 Hz), but the spacing between bands (∼60–200 Hz) is comparable to that observed on FAST and is always less than f_{cp}, ranging from 0.1 to 0.55 f_{cp} with most observations near 0.2 f_{cp}. This implies that if the waves are generated at harmonics of the proton gyrofrequency, they would have to be generated at a considerably higher altitude than DEMETER, but at altitudes comparable to those implied by the FAST observations. Waves such as these, electromagnetic waves at harmonics of the proton gyrofrequency, have been shown to propagate freely from such a source region, across L-shells and down to DEMETER altitudes [*Lund and LaBelle*, 1997; *Parrot et al.*, 2006a].

[31] To investigate whether ion bands consistent with those observed concurrently with the banded waves could be responsible for the wave growth at these frequencies, we used modeled banded ion distributions as input to the WHAMP code [*Rönnmark*, 1982] and looked for wave growth near the ion gyrofrequency and its harmonics. For a given input particle distribution, one can use the WHAMP code to look at wave growth (or decay) on any wave mode surface in any given frequency range. The input particle distributions used in this study are listed in Table 2. To model a single ion band (or ring in velocity space) distribution, we use two ion species, one of positive and one of negative density (both 10 cm^{-3}), with the positive density population having a temperature of 950 eV and the negative having a temperature of 150 eV. Figure 13 (right) shows the ion energy flux of this model particle distribution (for H^+ ions) with parallel energy on the *x* axis and perpendicular energy on the *y* axis, both from -10^8 to 10^8 eV. For comparison, Figure 13 (left) shows the actual ion flux from the FAST data at 05:07:30 on 08-30-1998, a time taken from the interval shown in Figures 5–8 during which there was one

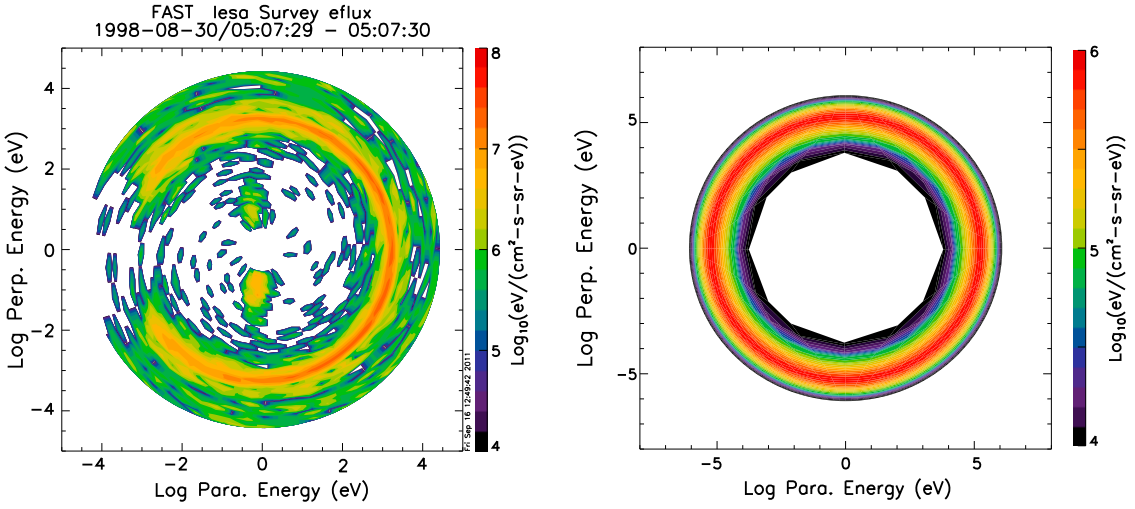

Figure 13. (left) Polar plot of ion energy flux, with parallel and perpendicular energy on the x- and y-axes in log format. (right) Ion energy flux of model particle distribution for a single H^+ ion band, using two ion species, one of positive and one of negative density (both 10 cm^{-3}), with the positive density population having a temperature of 950 eV and the negative having a temperature of 150 eV (see Table 2).

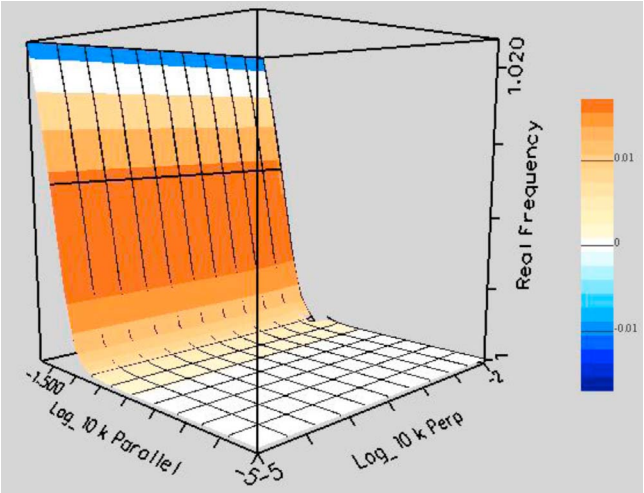

Figure 14. WHAMP output using the distribution shown in Figure 10 as input. The z axis is frequency in units of the proton gyrofrequency from 1 to 1.022, and the color scale shows wave growth from −0.02 (blue) to 0.02 (brown). Wave growth is seen in a narrow band just above the proton gyrofrequency, with growth rates of ∼0.01–0.02 times the proton gyrofrequency.

particularly intense ion band. The model is not intended to exactly replicate the observations, but the single strong ion band is evident in both plots. Note that there is also a single loss cone in the observed data, which is not included in the model.

[32] Figure 14 shows the WHAMP results for the distribution shown in Figure 13 (right). The z axis in Figure 14 is frequency in units of the proton gyrofrequency from 1 to 1.022, and the color scale shows wave growth from −0.02 (blue) to 0.02 (brown). Wave growth is seen in a narrow band just above the proton gyrofrequency, with growth rates of ∼0.01–0.02 f_{cp}. This represents significant wave growth, consistent with the generation of a band of wave emissions as observed. The wave polarization at an oblique angle to the ambient magnetic field is consistent with the observations shown in Figure 9. The E/B ratio for the resulting waves is $\sim 10^6$–10^7, comparable to the observed waves and consistent with electromagnetic emissions. Additionally, the slope of the wave surface implies electromagnetic waves capable of propagation, consistent with the observation of these banded waves in both the electric and magnetic field, and with their persistence for several hours at a range of altitudes, L-shells, and latitudes. Similar wave growth is also observed at higher harmonics of the proton gyrofrequency (not shown). Wave growth specifically at harmonics closest to the lower hybrid frequency, such as that observed, involves coupling between the ion Bernstein and lower hybrid instabilities and is not replicable using the WHAMP code. However, the WHAMP results serve to illustrate that banded ions can generate waves at ion gyroharmonics. Independent simulations by *Gary et al.* [2011] demonstrate that similar ion distributions, with a hot velocity ring component derived from storm time observations and ring current models, generate obliquely propagating electromagnetic waves at harmonics of the proton gyrofrequency, including the higher harmonics such as those reported here.

[33] The multiple energy band ions can be modeled by adding additional components to the WHAMP input. The WHAMP output for an input of two proton rings is shown in Figure 15. This additional ion band reduces the growth in this wave band to 0.002–0.004 f_{cp}, but otherwise the results are the same. In the FAST data, there are observations of both single and multiple ion bands, and the WHAMP results support the idea that these bands could generate banded waves similar to those observed. The addition of ion bands of other species such as oxygen provides more free energy and allows for wave growth at other, lower frequencies. Specifically, the addition of an oxygen band with the same temperature and density as the proton band shown in Figure 13 results in the same wave growth at the proton cyclotron frequency as well as a narrow band of wave growth (about 0.01–0.02 f_{co}) in the frequency band f = (1–1.12) f_{co}, where f_{co} is the oxygen cyclotron frequency given by $f_{co} = 0.0625\ f_{cp}$.

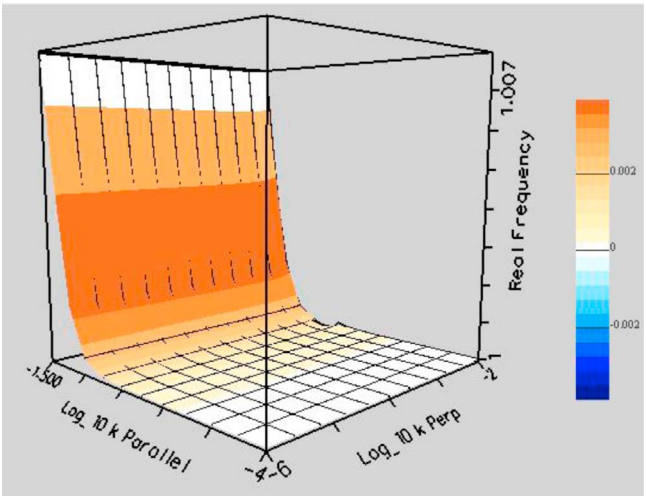

Figure 15. WHAMP output for an input of two proton rings (see Table 2). This additional ion band reduces the growth in this wave band to 0.002–0.004 times the proton gyrofrequency, but otherwise the results are the same.

However, as most of the observed energy flux is in the proton bands and waves at frequencies in this lower range are not observed, it is likely the free energy in the proton distribution is the source responsible for wave growth in the observed bands.

5. Conclusions

[34] Electromagnetic VLF emissions in the frequency range ~75–2000 Hz, appearing as discrete frequency bands between separated by 60–200 Hz, are observed independently on the FAST and DEMETER satellites during very strong geomagnetic storms. The VLF emissions are coincident with FAST observations of warm energy-banded ions in the low latitude auroral and sub-auroral zone. These banded emissions persist for several orbits, lasting up to 12 h, in both the northern and southern hemispheres. The emissions are evident in both the electric and magnetic fields, with E/B $\sim 10^5$ m/s for both the FAST and DEMETER observations. The banded wave observations are correlated with ion and electron density enhancements, i.e., the waves are observed during enhancements in the density and drop out when the density decreases. These waves could play a role in energy transfer between particle populations, ion heating, and mass outflow during large geomagnetic storms.

[35] These banded waves are observed coincident with energy-banded ions, suggesting that free energy in the ion distributions may be responsible their generation. The FAST wave observations, close to the inferred source region, are near the lower hybrid frequency, so the mechanism proposed by *Cattell and Hudson* [1982] where a coupling between the lower hybrid instability and ion Bernstein modes was found to generate electrostatic banded waves near the lower hybrid frequency, is likely to be involved in the generation of the waves observed here. This coupling could explain why the lower harmonics of f_{ci}, far from f_{lh}, are not observed. Both the FAST and DEMETER observations include a significant magnetic wave component, with an E/B ratio of $\sim 10^5$ m/s, consistent with electromagnetic emissions unlike the electrostatic waves investigated by *Cattell and Hudson* [1982], but in both cases banded waves are observed most intense around f_{lh} in the inferred source region, implying the same coupling mechanism is responsible for the generation of the waves.

[36] Banded electromagnetic waves similar to those observed on FAST and DEMETER have been shown to arise from free energy in a proton velocity ring distribution by *Gary et al.* [2011], who refer to these waves as proton Bernstein waves, and discuss the difficulties associated with inconsistent nomenclature in the literature for waves observed in different areas of the magnetosphere. As such, we refer to the emissions reported herein simply as banded electromagnetic emissions; though the observed waves are oblique EM waves like those shown in the *Gary et al.* [2011] simulations, they represent a new phenomenon, distinct from previous observations. Using model particle distributions of banded ions similar to those observed on FAST at the same time as the wave observations, the calculated wave growth at harmonics of the source region proton gyrofrequency was significant, suggesting that these emissions could be generated by the observed ions. To match harmonics of the local proton gyrofrequency in the source region, these waves would have to be generated just above ~4000 km, above the location of both satellites; such waves have previously been shown to be capable of propagating to the spacecraft locations.

[37] These emissions are observed on two different satellites, which were operating in two different locations under different plasma conditions. Given the limited range in both latitude and altitude covered by these satellites, it is impossible to definitively state that the waves observed on DEMETER and FAST arise from the same source. However, their similar frequency range, frequency-time structure, and E/B values, together with their coincidence with energy-banded ions and occurrence during the strongest magnetic storms, suggests that they are examples of the same phenomenon. We put forth that the banded ion distribution, and the free energy therein, generates waves at harmonics of the local proton gyrofrequency. Coupling with the lower hybrid instability causes the bands closest to f_{lh} to appear more intense, and the waves then propagate to the spacecraft locations where they are observed. It should be noted that the persistence of the banded ions over several orbits, coupled with the intermittent nature of the banded wave emissions during these intervals, suggests that the banded ion distribution is a necessary but not sufficient condition for the generation of these waves. Further investigation into the nature of the instability will be carried out to examine the details of their generation mechanism.

[38] **Acknowledgments.** The authors thank Richard Denton and Susan Schwartz for access to the WHAMP code. The DEMETER satellite is supported by the French Centre National d'Etudes Spatiales, and the authors thank J.J. Berthelier and J.P. Lebreton for the use of the DEMETER data. This work was supported by NASA grants NNX09AV48G, NNG04GP84G, and NNX10AL03G.

[39] Masaki Fujimoto thanks the reviewers for their assistance in evaluating this paper.

References

André, M., M. Temerin, and D. Gorney (1986), Resonant generation of ion waves on auroral field lines by positive slopes in ion velocity space, *J. Geophys. Res.*, *91*(A3), 3145–3151, doi:10.1029/JA091iA03p03145.

Baumgardner, J., J. Wroten, J. Semeter, J. Kozyra, M. Buonsanto, P. Erickson, and M. Mendillo (2007), A very bright SAR arc: Implications for extreme magnetosphere-ionosphere coupling, *Ann. Geophys.*, *25*, 2593–2608, doi:10.5194/angeo-25-2593-2007.

Berthelier, J. J., et al. (2006a), ICE, The electric field experiment on DEMETER, *Planet. Space Sci.*, *54*, 456–471, doi:10.1016/j.pss.2005.10.016.

Berthelier, J. J., M. Godefroy, F. Leblanc, E. Seran, D. Peschard, P. Gilbert, and J. Artru (2006b), IAP, the thermal plasma analyzer on DEMETER, *Planet. Space Sci.*, *54*, 487–501, doi:10.1016/j.pss.2005.10.018.

Boehm, M., D. Klumpar, E. Möbius, L. Kistler, J. McFadden, C. Carlson, and R. Ergun (1999), FAST auroral snapshot observations of bouncing ion distributions: Fieldline length measurements, *J. Geophys. Res.*, *104*, 2343–2355, doi:10.1029/98JA02290.

Burtis, W., and R. Helliwell (1969), Banded chorus—A new type of VLF Radiation observed in the magnetosphere by OGO 1 and OGO 3, *J. Geophys. Res.*, *74*(11), 3002–3010, doi:10.1029/JA074i011p03002.

Carlson, C. W., J. P. McFadden, P. Turin, D. W. Curtis, and A. Magoncelli (2001), The electron and ion plasma experiment for Fast, *Space Sci. Rev.*, *98*, 33–66, doi:10.1023/A:1013139910140.

Cattell, C., and M. Hudson (1982), Flute mode waves near ω_{LH} excited by ion rings in velocity space, *Geophys. Res. Lett.*, *9*(10), 1167–1170, doi:10.1029/GL009i010p01167.

Cattell, C., et al. (2002), FAST observations of discrete electrostatic waves in association with down-going ion beams in the auroral zone, *J. Geophys. Res.*, *107*(A9), 1238, doi:10.1029/2001JA000254.

Cattell, C. A., M. F. Thomsen, J. Kozyra, B. Lavraud, J. Borovsky, and J. Dombeck (2004), Energized banded ions during large geomagnetic

storms: Comparisons of observations at geosynchronous and low altitudes, *Rep. COSPAR-04-A-02925*, Comm. on Space Res, Paris.

Chaston, C. C., J. W. Bonnell, J. P. McFadden, R. E. Ergun, and C. W. Carlson (2002), Electromagnetic ion cyclotron waves at proton cyclotron harmonics, *J. Geophys. Res.*, *107*(A11), 1351, doi:10.1029/2001JA900141.

Dandouras, I., J. Cao, and C. Vallat (2009), Energetic ion dynamics of the inner magnetosphere revealed in coordinated Cluster-Double Star observations, *J. Geophys. Res.*, *114*, A01S90, doi:10.1029/2007JA012757.

Elphic, R. C., J. D. Means, R. C. Snare, R. J. Strangeway, L. Kepko, and R. E. Ergun (2001), Magnetic field instruments for the Fast Auroral Snapshot Explorer, *Space Sci. Rev.*, *98*, 151–168, doi:10.1023/A:1013153623344.

Ergun, R. E., et al. (2001), The FAST satellite fields instrument, *Space Sci. Rev.*, *98*, 67–91, doi:10.1023/A:1013131708323.

Gary, S. P., K. Liu, and D. Winske (2011), Bernstein instability driven by suprathermal protons in the ring current, *J. Geophys. Res.*, *116*, A08215, doi:10.1029/2011JA016543.

Hamilton, D. C., G. Gloeckler, F. M. Ipavich, W. Studemann, B. Wilken, and G. Kremser (1988), Ring current development during the great magnetic storm of February 1986, *J. Geophys. Res.*, *93*(A12), 14,343–14,355, doi:10.1029/JA093iA12p14343.

Hirahara, M., A. Yamazaki, K. Seki, T. Mukai, E. Sagawa, N. Kaya, and H. Hayakawa (1997), Characteristics of downward flowing ion energy dispersions observed in the low-altitude central plasma sheet by Akebono and DMSP, *J. Geophys. Res.*, *102*(A3), 4821–4839, doi:10.1029/96JA03332.

Huang, C. Y., W. J. Burke, and C. S. Lin (2005), Ion precipitation in the dawn sector during geomagnetic storms, *J. Geophys. Res.*, *110*, A11213, doi:10.1029/2005JA011116.

Kintner, P. M. (1980), On the distinction between electrostatic ion cyclotron waves and ion cyclotron harmonic waves, *Geophys. Res. Lett.*, *7*(8), 585–588, doi:10.1029/GL007i008p00585.

Klumpar, D. M., et al. (2001), The Time-of-Flight Energy, Angle, Mass Spectrograph (TEAMS) Experiment for FAST, *Space Sci. Rev.*, *98*, 197–219, doi:10.1023/A:1013127607414.

Koskinen, H. E. J., P. M. Kintner, G. Holmgren, B. Holback, G. Gustafsson, M. André, and R. Lundin (1987), Observations of ion cyclotron harmonic waves by the Viking satellite, *Geophys. Res. Lett.*, *14*(4), 459–462, doi:10.1029/GL014i004p00459.

Kozyra, J. U., A. F. Nagy, and D. W. Slater (1997), High-altitude energy source(s) for stable auroral red arcs, *Rev. Geophys.*, *35*(2), 155–190, doi:10.1029/96RG03194.

Kozyra, J. U., et al. (2004), Coupling processes in the inner magnetosphere associated with midlatitude red auroras during superstorms, *Eos Trans. AGU*, *85*(47), Fall Meet. Suppl., Abstract SM12B-03.

Lebreton, J. P., et al. (2006), The ISL Langmuir Probe experiment and its data processing onboard DEMETER: Scientific objectives, description and first results, *Planet. Space Sci.*, *54*, 472–486, doi:10.1016/j.pss.2005.10.017.

Liu, H., S. Kokubun, and K. Hayashi (1994), Equatorial electromagnetic emission with discrete spectra near harmonics of oxygen gyrofrequency during magnetic storm, *Geophys. Res. Lett.*, *21*(3), 225–228, doi:10.1029/93GL02836.

Lund, E. J., and J. LaBelle (1997), On the generation and propagation of auroral electromagnetic ion cyclotron waves, *J. Geophys. Res.*, *102*(A8), 17,241–17,253, doi:10.1029/97JA01455.

McFadden, J. P., Y. K. Tung, C. W. Carlson, R. J. Strangeway, E. Moebius, and L. M. Kistler (2001), FAST observations of ion outflow associated with magnetic storms, in *Space Weather*, *Geophys. Monogr. Ser.*, vol. 125, edited by P. Song, H. J. Singer, and G. L. Siscoe, pp. 413–421, AGU, Washington, D. C., doi:10.1029/GM125p0413.

Němec, F., O. Santolík, M. Parrot, and J. J. Berthelier (2006), Power line harmonic radiation (PLHR) observed by the DEMETER spacecraft, *J. Geophys. Res.*, *111*, A04308, doi:10.1029/2005JA011480.

Němec, F., M. Parrot, O. Santolík, C. J. Rodger, M. J. Rycroft, M. Hayosh, D. Shklyar, and A. Demekhov (2009), Survey of magnetospheric line radiation events observed by the DEMETER spacecraft, *J. Geophys. Res.*, *114*, A05203, doi:10.1029/2008JA014016.

Parrot, M., A. Buzzi, O. Santolík, J. J. Berthelier, J. A. Sauvaud, and J. P. Lebreton (2006a), New observations of electromagnetic harmonic ELF emissions in the ionosphere by the DEMETER satellite during large magnetic storms, *J. Geophys. Res.*, *111*, A08301, doi:10.1029/2005JA011583.

Parrot, M., et al. (2006b), The magnetic field experiment IMSC and its data processing onboard DEMETER: Scientific objectives, description and first results, *Planet. Space Sci.*, *54*, 441–455, doi:10.1016/j.pss.2005.10.015.

Pfaff, R. F., Jr., C. Liebrecht, J.-J. Berthelier, M. Malingre, M. Parrot, and J.-P. Lebreton (2008), DEMETER satellite observations of plasma irregularities in the topside ionosphere at low, middle, and sub-auroral latitudes and their dependence on magnetic storms, in *Midlatitude Ionospheric Dynamics and Disturbances*, *Geophys. Monogr. Ser.*, vol. 181, edited by P. M. Kintner, Jr. et al., pp. 297–310, AGU, Washington, D. C.

Rönnmark, K. (1982), WHAMP–waves in homogeneous, anisotropic multicomponent plasmas, *Rep. KGI-179*, Kiruna Geophys. Inst., Kiruna, Sweden.

Roth, I., and M. Hudson (1985), Lower hybrid heating of ionospheric ions due to ion ring distributions in the cusp, *J. Geophys. Res.*, *90*(A5), 4191–4203, doi:10.1029/JA090iA05p04191.

Roth, I., C. Carlson, M. Hudson, and R. Lysak (1983), Simulations of beam excited minor species gyroharmonics in the Porcupine experiment, *J. Geophys. Res.*, *88*(A10), 8115–8122, doi:10.1029/JA088iA10p08115.

Swider, W. (1990), Precipitating and trapped ions and electrons observed at 840 km during the great magnetic storm of February 1986, *J. Geophys. Res.*, *95*(A7), 10,417–10,425, doi:10.1029/JA095iA07p10417.

Titova, E. E., A. G. Demekhov, D. L. Pasmanik, V. Y. Trakhtengerts, J. Manninen, T. Turunen, and M. J. Rycroft (2007), Ground-based observations at L ∼6 of multi-band structures in VLF hiss, *Geophys. Res. Lett.*, *34*, L02112, doi:10.1029/2006GL028482.

Yao, Y., K. Seki, Y. Miyoshi, J. P. McFadden, E. J. Lund, and C. W. Carlson (2008), Statistical properties of the multiple ion band structures observed by the FAST satellite, *J. Geophys. Res.*, *113*, A07204, doi:10.1029/2008JA013178.

Zhang, Y., L. J. Paxton, J. U. Kozyra, H. Kil, and P. C. Brandt (2006), Nightside thermospheric FUV emissions due to energetic neutral atom precipitation during magnetic superstorms, *J. Geophys. Res.*, *111*, A09307, doi:10.1029/2005JA011152.